Using Fluid Curtains to Improve Sealing Performance in Turbomachinery Applications

J.A. MacCalman, R.J. Williams, G.L. Ingram & S.I. Hogg

Department of Engineering, Durham University, Durham, UK, DH1 3LE.

Abstract

The results from an investigation into the physics of how fluid curtains can be applied to improve the aerodynamic performance of conventional turbomachinery shaft and rotor seals are described in this paper. Computational fluid dynamics and testing on two experimental facilities are used in the study. In the first part of the work, computational fluid dynamics simulations validated against experimental test data demonstrate the fundamental mechanism by which the presence of the curtain can act to reduce leakage flow through conventional seals. These results are consolidated into a single performance carpet map, showing how the leakage reduction performance and the curtain supply pressure needed to achieve it vary with changes in values of key geometrical parameters. In the second part of the work the effect of swirl in the seal inlet flow, as is often encountered in turbomachinery applications, on the performance of the fluid curtain is investigated experimentally. Test results show that if the swirl momentum in the inlet flow is greater than the momentum of the curtain flow, the performance benefit from applying the curtain is greatly diminished. Overall, the results provide some fundamental design rules for applying fluid curtains to enhance turbomachinery sealing performance for the general type of leakage path geometry (cylindrical channel, 45-degree jet angle, curtain upstream of a conventional seal) and working fluid type and conditions (air, ambient temperature, subsonic leakage channel flow), used in the study.

Nomenclature

a	Fluidic curtain width	(mm)
b	Leakage channel height	(mm)
c	Labyrinth seal clearance height	(mm)
d	Spacing between curtain inlet and labyrinth seal	(mm)
A	Ratio of b to a	(-)
C	Ratio of b to c	(-)
D	Ratio of d to b	(-)
L	Percentage reduction in leakage flow rate	(-)
$\dot{m}$	Mass flow rate	(kg/s)
P_0	Total pressure	(bar)
P	Static pressure	(bar)
PR	Pressure ratio	(-)
v	Velocity	(m/s)
ρ	Density	(kg/m^3)

Introduction

In recent decades, much of the innovation in new internal turbomachinery sealing technology to achieve performance levels above that of conventional labyrinth seals (Figure 1 (a)) has been focussed on developing concepts that feature compliant physical barriers to restrict leakage flows, such as brush seals [1] (Figure 1 (b)), finger seals [2] and leaf seals [3]. These new seal types are designed to be more tolerant of shaft rubbing compared to conventional labyrinth seals [4]. The challenges associated with developing new types of robust seal of this nature with the design life needed to make them realistic high-performance replacements for labyrinth seals is now recognised and work is ongoing to try to address this [5,6]. In contrast, as noted by Curtis et. al. [7], the concept

of using fluid jets or curtains (Figure 1 (c)) to reduce turbomachinery leakage flow has received relatively little attention in the open literature. Some recent examples of studies include [8] and [9] but they still remain relatively few in number, which is surprising considering that there is no fundamental barrier preventing application in turbomachinery. Ideas for using this type of device for reducing leakage can be found mainly in patents, some dating back over 50 years. Auyer [10] published a patent in 1954 that described using inclined jets over an unshrouded turbine blade row to reduce over-tip leakage. A patent by Smile & Paulson [11] in 1960 concerns applying an auxiliary pressurised cavity above a shrouded turbine rotor to reduce leakage. Unsworth and Burton [12] were granted a patent in 1971 for using inclined jets above a shrouded rotor to reduce leakage. Minoda et al. [13] describe applying an array of radial jets above an unshrouded rotor to control leakage in their 1988 patent. In 2009, Turnquist et al. [14] patented a range of ideas for applying fluid jets to reduce leakage through both shaft gland seals and turbine rotor tip seals.

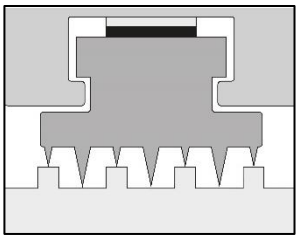

(a) Conventional multi-fin stepped labyrinth (castellated) seal design applied to a shaft seal.

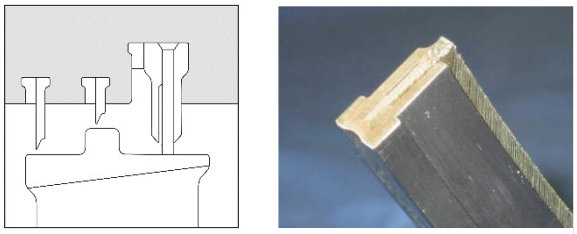

(b) Labyrinth seal and brush seal (picture) combined on a rotor blade tip seal.

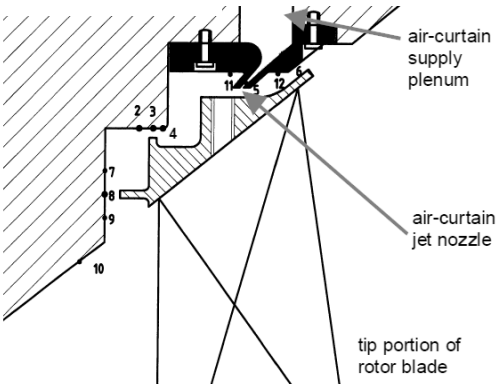

(c) Rotor blade tip seal design with fluid curtain tested by Curtis et al [7].

Figure 1: Different seal designs for turbomachinery applications.

Curtis et. al. [7] presented the first rigorous experimental and computational study that demonstrated the potential of air curtain sealing on a turbine tip seal application, in their award-winning paper from the 2009 ASME Turbo Expo Conference. In this paper they describe a study where a fluid curtain was applied to the tip seal of a shrouded low pressure turbine blade. Experiments were carried out on a single stage model turbine test facility with guide vanes upstream and downstream of the test stage to condition the inlet and exit flows. The results showed that overall efficiency improvements (including correction for the ideal work that the air-curtain flow could provide) of up to 0.5% could be achieved for the stage tested.

The model turbine test stage used by Curtis et. al. [7] was for a single turbine stage geometry that was characterised by a large change in radius in the flow through the stage resulting in the rotor tip shroud having a flare-angle of approximately 45 degrees. The rotor tip seal design featured a radial clearance seal restriction and an axial restriction in addition to the fluid curtain to control the leakage flow. The concept of using a fluid curtain to augment the sealing performance of other types of turbomachinery seal is explored further in this paper. A parametric study of an idealised seal geometry incorporating a fluid curtain has been conducted which, for the first time, provides an insight into the effectiveness of fluid curtains in reducing total seal leakage over a design space characterised by a small number of dimensionless geometric parameters. CFD predictions validated against experiments are used to produce a performance map, which shows how the optimum leakage reduction performance and the curtain supply pressure needed to achieve it, vary with changes in values of the key geometrical parameters. In a second part of the work, the effect of swirl in the leakage inlet flow, which is often encountered in turbomachinery applications, is investigated experimentally. The results are the first demonstration of the detrimental impact that higher levels of swirl momentum in the inlet flow compared to the momentum of the fluid curtain can have on the ability of the curtain to reduce total leakage flow through the seal.

The fundamental physics of how fluid curtain seals can be applied to reduce the net leakage exiting a labyrinth seal is shown in Figure 2.

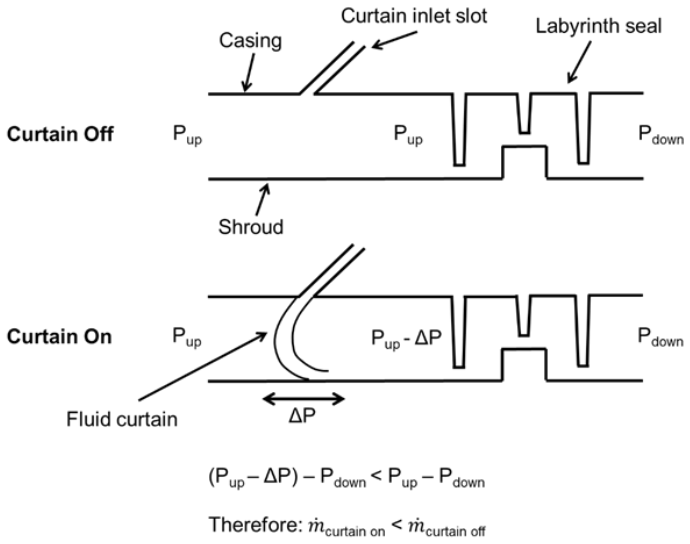

Figure 2: Fundamental physics of how fluid curtains can be applied to reduce leak through turbomachinery seals.

Figure 2 shows an idealised diagram of a stepped labyrinth seal featuring 3 restrictions in the leakage channel between stationary (casing) and rotating (shroud) surfaces, as is typically encountered in turbomachinery applications. The aim of the seal is to minimise the leakage flow along the leakage channel which enters at inlet static pressure P_{up} and exits at a lower seal exist static pressure P_{down}. The upper diagram in Figure 2 shows the sealing arrangement with the fluid curtain flow turned off. In this state, assuming inviscid flow, the static pressure immediately before the first labyrinth seal restriction will be equal to the seal inlet static pressure, P_{up} , and the full pressure drop between the leakage channel inlet and exit pressures will be driving flow through the labyrinth seal. The lower diagram in Figure 2 shows the effect of turning the fluid curtain flow on. The fluid curtain enters the channel at an angle in the opposite direction to the leakage flow through the channel. The fluid

curtain flow therefore opposes the leakage flow in the channel. Provided that the momentum of the fluid curtain flow is not too great, the channel leakage flow will act to turn the curtain flow to align it with its direction, as shown in the diagram. There must be a static pressure drop, ΔP, in the channel where the turning of the curtain flow occurs to affect its change of direction. The static pressure immediately upstream of the first labyrinth restriction is now reduced to (P_{up} - ΔP) and consequently the static pressure drop driving the flow through the labyrinth seal has been reduced by ΔP. The flow exiting from the leakage channel after the labyrinth seal will be the sum of the curtain flow plus any flow across the leakage channel inlet boundary. The reduction in pressure drop across the labyrinth seal caused by the fluid curtain results in a leakage flow exiting the leakage channel with the curtain applied that must be less than the leakage flow through the channel with the curtain turned off. The effect of the leakage flow reduction on thermal efficiency will depend upon the thermodynamic state of the flow supplying the fluid curtain and the ideal work that would otherwise be available from it. It is not automatically the case that using a fluid curtain to reduce leakage mass flow will lead to an improvement in overall thermal efficiency of a turbine stage. Curtis et. al. [7] provide a demonstration of an externally supplied fluid curtain being used successfully to reduce tip leakage flow and to improve the overall thermal performance of a turbine stage. It should be noted that their experiments demonstrate that the maximum efficiency benefit from applying the fluid curtain occurs at a different operating condition (lower curtain flow) than that needed for zero leakage flow through the tip seal. Optimising the use of fluid curtains to reduce leakage flow and improve thermal performance of a turbomachine will depend upon the application and the design intent (i.e. minimising leakage or maximising efficiency). A thermodynamic analysis of the complete system will be required to determine the effect on overall efficiency. Finally, the optimum leakage reduction performance will be achieved when the momentum of the fluid curtain flow is just sufficient to prevent any flow from entering the leakage channel through its inlet. If the momentum of the fluid curtain is increased beyond this level, some of the curtain flow will flow out of the

channel through its inlet mixing with the main stage flow at the inlet to the rotor. This will cause a performance loss. This was also demonstrated in the results by Curtis et. al. [7].

The work described in this paper is a fundamental study of the physics behind the aerodynamics of using fluid curtains to improve seal performance. The results from the study provide the first set of design guidelines for incorporating fluid curtains into turbomachinery seal designs to improve performance through reduced leakage flow. The work is divided into two parts. The first part describes a study to understand the values of fundamental dimensionless parameters that define jet thickness, effective seal clearance and jet supply pressure, which result in significant leakage reduction from applying a fluid curtain. The CFD used to generate the parameter maps is validated against experimental data. The second part of the paper describes experiments that were undertaken to investigate the impact of swirl in the inlet flow on the performance of the fluid curtain. Swirl is often found to impact on the performance of turbomachinery seals. For example, in multi-fin labyrinth seals swirl in the leakage flow can sometimes result in destabilising rotordynamic forces that lead to shaft whirl in extreme cases [15]. For brush seals, swirl can cause large amplitude vibrations of the brush seal's bristles resulting in rapid bristle pack failure [6].

Optimising Seal Leakage Performance by Incorporating Fluid Curtains.

The idealised two-dimensional seal geometry shown in Figure 3 is used in this part of the study. The leakage performance of any type of turbomachinery seal (multi-fin labyrinth, brush seal, leaf seal, finger seal etc) can be modelled as a single labyrinth fin seal with a clearance set equivalent to the 'effective' clearance of the seal being modelled. The concept of an effective clearance as defined in [16], has been used extensively in studies when comparing the performance of different seals. The idealised geometry in Figure 3 can be used to investigate the fundamental effect on aerodynamic performance from including a fluid curtain upstream of any type of turbomachinery seal. The fluid

curtain has thickness ‘a’. It enters the leakage channel, which has constant height ‘b’, through the upper wall of the channel at a distant ‘d’ upstream of the single labyrinth restriction. A kinetic energy blocker is positioned on the lower channel wall mid-way between the curtain entry plane and the labyrinth restriction. It is well known that kinetic energy carry-over can adversely impact on the performance of multi-restriction labyrinth seals. This occurs when the kinetic energy in the flow underneath a restriction is not fully dissipated before the flow is required to accelerate underneath the next labyrinth restriction. One solution to this is the stepped (castellated) labyrinth design shown in Figure 1(a). This is a common design feature often used to prevent carry-over by avoiding two adjacent restrictions having the same radius. Kinetic energy carry-over from the fluid curtain to the labyrinth restriction is a risk for the geometry in Figure 3, so the ‘blocker’ (essentially equivalent to a castellation in a stepped labyrinth seal) has been introduced to prevent this. Finally, the fluid curtain is inclined at an angle of 45 degrees against the channel leakage flow. An angle closer to the normal will be less effective as less of the curtain momentum will be directed against the leakage flow in the channel. Higher angles would improve the aerodynamic effectiveness of the curtain but would be more challenging to manufacture and implement in designs. For these reasons, only the one curtain angle is used throughout this study. The full list of constraints in this part of the study are:

1. Curtain angles is 45 degrees.
2. Leakage path is a cylindrical channel of low radius ratio.
3. The fluid curtain is upstream of the seal element(s).
4. Subsonic leakage channel flow.
5. Working fluid air.
6. The ambient temperature is 20 degrees Celsius.
7. Zero swirl conditions.

The following dimensionless parameters are used to characterise the performance improvement from applying fluid curtains.

$$A = \frac{b}{a} \tag{1}$$

$$C = \frac{b}{c} \tag{2}$$

$$D = \frac{d}{b} \tag{3}$$

$$PR = \frac{P_{0,curtain} - P_{outlet}}{P_{0,inlet} - P_{outlet}} \tag{4}$$

$$L = \frac{\dot{m}_{outlet,no\ curtain} - \dot{m}_{outlet,with\ curtain}}{\dot{m}_{outlet,no\ curtain}} \tag{5}$$

The first 3 parameters define the seal geometry. A is the ratio of channel height to fluidic curtain thickness (Figure 3). C is the ratio of channel height to effective single labyrinth fin clearance. D is the ratio of the leakage channel distance between fluidic curtain inlet slot and the labyrinth fin compared to the channel height. The dimensionless curtain supply pressure, PR, is defined as the difference between the total pressure supplying the curtain flow and the leakage channel exit static pressure, divided by the total to static pressure drop between the inlet and the exit of the leakage channel. Finally, L, is the leakage reduction factor due to the presence of the fluid curtain.

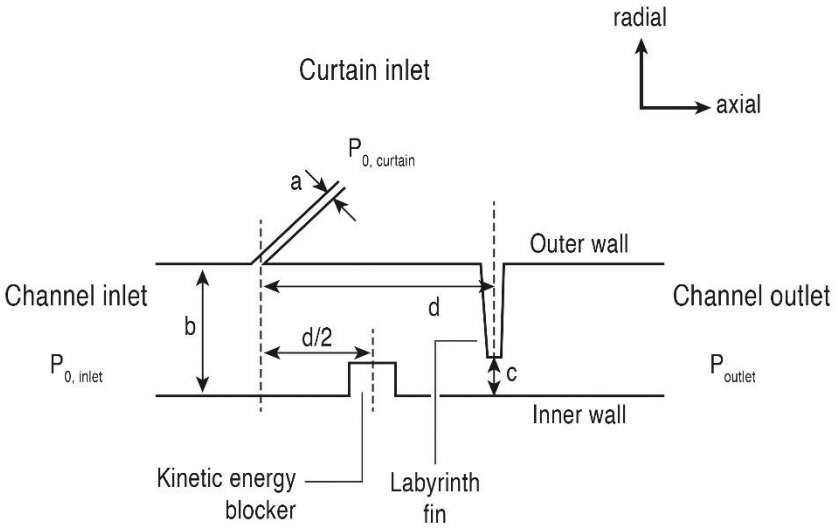

Figure 3: Idealised two-dimensional seal geometry incorporating a fluid curtain.

A test facility using air was constructed to investigate the influence of the parameters defined by Equations 1 to 4 on the performance of the fluid curtain with the idealised seal geometry. The aim of the experiments was to demonstrate the fluid curtain effect in operation and to generate test data for validating later CFD calculations.

Figure 4 shows a diagram of the test facility. The Durham Blowdown Tank was used to supply the test rig with air to test the seal designs. This facility consists of a 10m^3 refillable tank of compressed air. The tank was connected to the test facility by a system of 50mm galvanised steel pipes and was pressurised to 15bar before each test. The test rig inlet pressures (air curtain and leakage channel) needed to conduct each test were much lower than the starting air pressure in the tank. An automatically controlled governing valve in the line from the tank was used to regulate the air supply pressure before the test rig which allowed constant pressure test conditions to be maintained as the pressure in the Blowdown Tank fell. This arrangement provided run times of several minutes' duration during which the control valves were set to achieve the desired test rig inlet conditions and the test data was logged. The pipework was split before the test rig into two 25 mm diameter pipes providing independent supplies for the leakage channel inlet flow and the air curtain flow. Manually

operated control valves were used to control the pressures of both supplies. The leakage channel exit flow exhausted directly to atmosphere and so this pressure was the atmospheric pressure measured on the day in all tests.

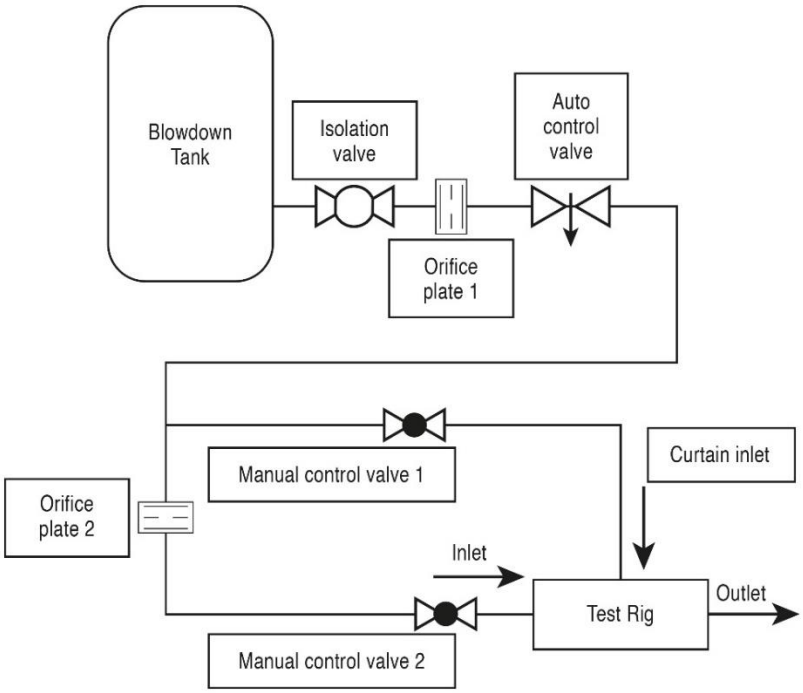

Figure 4: Schematic Diagram of the Static Test Rig Configuration for the Fluid Curtain Tests.

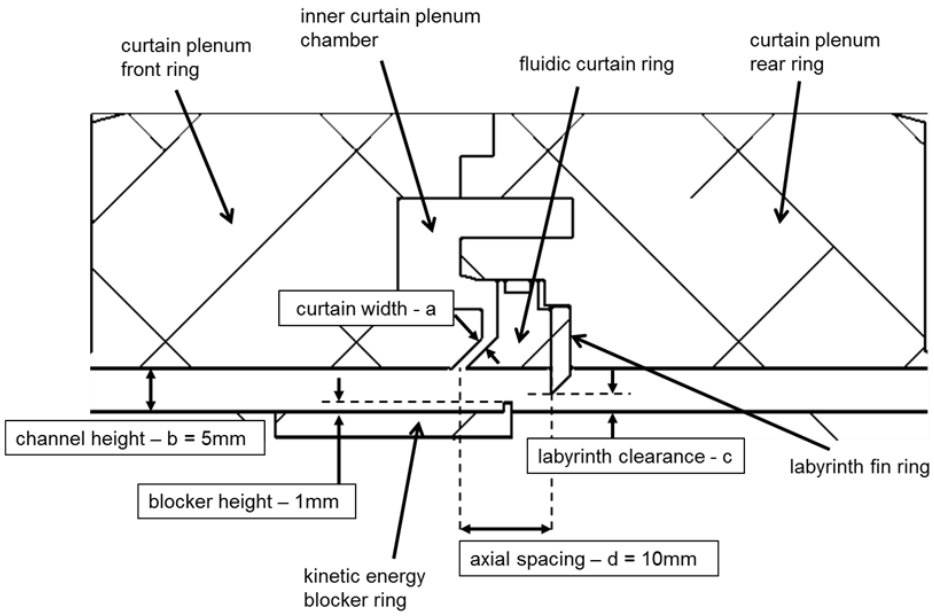

Figure 5: Idealised Seal Design Test Rig Working Section.

Orifice plate 1 in Figure 4 was used to measure the total mass flow to the test rig (i.e. leakage channel inlet flow plus the curtain flow). Orifice plate 2 was used to measure the leakage channel inlet mass flow rate. The fluidic curtain mass flow rate was not measured directly but was determined from the difference between the two orifice plate measurements. The orifice plates designs used conformed to the British Standard; ISO:5167:2003. Appropriately rated Sensor Technics pressure transducers with accuracies of 0.2% FSO or better were used to measure the absolute and differential orifice plate pressures. Uncertainty in the mass flow rate measurements from the orifice plates was calculated according to BS EN ISO 5167-1:2003 and found to be less than 2% for the range of test conditions used.

Figure 5 shows a diagram of the working section of the test rig (axisymmetric design), including some of its key dimensions. The test rig consisted of a set of concentric annular steel components held together by a ring of threaded steel tie bars. A central stationary cylindrical shaft formed the inner surface of the leakage channel. Air from the blowdown tank was supplied to the inner curtain plenum chamber (connections not shown) and to a separate plenum connecting to the leakage channel inlet (not shown). The leakage channel height, b, used in the tests was 5 mm and the channel was 115 mm long. The diameter of the cylinder forming the inner wall was 80 mm giving a radius ratio of 1.125 for the leakage channel outer to inner walls. The axial distance, d, from the air curtain inlet plane to the labyrinth seal fin was 10 mm (i.e. D = 2 using Equation 3) in all tests. The labyrinth fin consisted of a steel ring with the inner bore chamfered at 45 degrees to a knife-edge. The ring was clamped between the fluid curtain ring and the curtain plenum rear ring, as show in Figure 5. This arrangement allowed the labyrinth fin clearance, c, to be changed during testing by changing the labyrinth fin ring for an alternative design with a different inner diameter. The air curtain was formed by a conical channel between the fluid curtain ring and the curtain plenum front ring. The air curtain thickness (width), a, was changed in the testing by placing metal shims (not

shown in Figure 5) between the labyrinth fin ring and the curtain plenum rear ring, allowing the location of the fluid curtain ring to be moved axially relative to the curtain plenum front ring. Tests were carried out using curtain thicknesses ranging from 0.29mm to 0.84mm and labyrinth fin clearances of 2mm and 2.5mm. A square section kinetic energy blocker with a height of 1 mm located at d/2 was used in all of the tests. The blocker was machined onto a split ring located in a groove in the leakage channel inner wall cylinder. Grub screws were used to hold the split ring halves in place during testing.

A Scanivalve Corp DSA3217 Digital Sensor Array was used to measure pressure data in the tests rig. This sensor array has an accuracy of 0.05% FSO. All of the pressure signals (test data and rig control signals) were logged using a National Instruments USB6218 data acquisition card. All test data was measured using the Scanivalve.

During testing, Manual Control Valve 2 (see Figure 4) was adjusted to ensure that the total pressure of the leakage channel inlet flow ($p_{0,inlet}$) was held constant at nominally 1.5 bara for all tests. The leakage channel outlet flow exhausts to atmosphere and so the static pressure at exit from the leakage channel (p_{outlet}) was the atmospheric pressure measured at the time of the test. Changes in the value of PR (Equation 4) were made in the testing by setting different positions for Manual Control Valve 1 to change the air curtain supply pressure and then adjusting Manual Control Valve 2 to return the leakage channel inlet total pressure to 1.5 bara.

During testing it was, of course, not possible to set the inlet plenum pressure (1.5 bara) and the curtain supply pressure to precisely match the target test conditions. Also, the tests were conducted over several days and so there was some variation in the leakage channel exit pressure (atmospheric pressure) during the testing. This resulted in differences between the desired and the actual test conditions used in the experiments. During post-processing of the test data, two-dimensional

(bilinear) interpolation was used to adjust the values of the measured leakage flows to (i) a standard leakage channel pressure drop of 0.5 bar (i.e. $p_{0,inlet}$ = 1.5 bara & p_{outlet} = 1.0 bara) and (ii) to the desired values for PR taking into account any change in atmospheric pressure for each test.

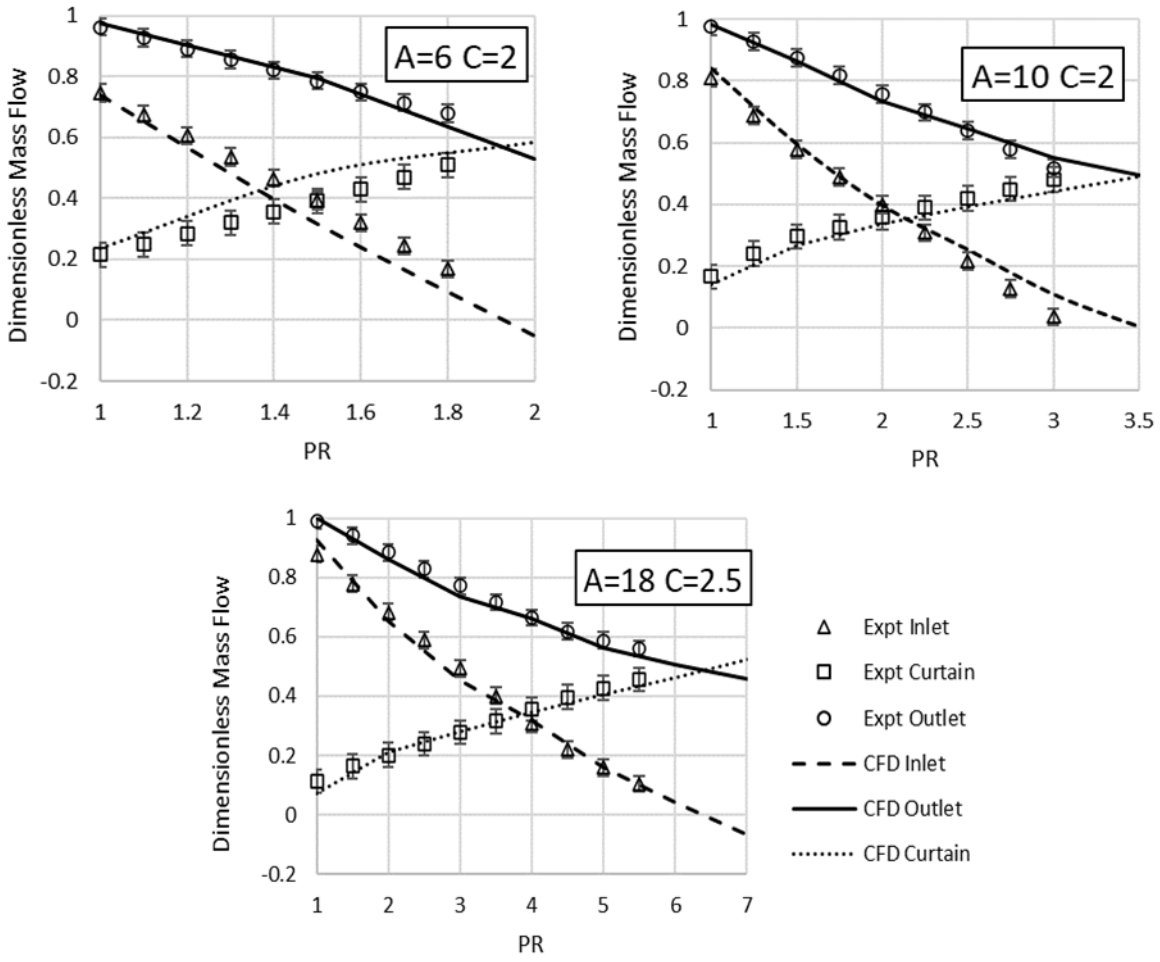

Figure 6: Experimental and CFD Results for Idealised Seal Geometry.

The test data shown in Figure 6 has been processed in this manner. The figure includes test results for three of the combinations of geometric parameters A and C tested. The error bars in the figure show the measurement uncertainty. The graphs show PR values on the horizontal axis and the leakage flows nondimensionalised by the flow through the leakage channel with the curtain switched off on the vertical axis.

The test results confirm the expected trends that are consistent with the fundamental physics of how the fluid curtain acts to reduce overall leakage flow, described earlier in relation to Figure 2. As expected, in all cases as the curtain strength (value of PR) is increased, the flow into the leakage channel is reduced by amounts greater than the curtain mass flow, resulting in a net overall leakage reduction at the channel outlet. It can be seen from Figure 6 that the curtain flow is not zero for PR = 1.0. This is because there will be flow along the leakage channel at this value of PR resulting in a static pressure in the channel at the location where the curtain enters the channel flow which is less than the leakage channel inlet total pressure and the total pressure in the plenum supplying the curtain flow. This results in the relatively small amount of curtain flow at this condition. It is also evident in Figure 6 that the experimental results stop before the value of PR needed to achieve the optimum sealing with zero flow through the leakage channel inlet. It is not possible to achieve test conditions where the flow reverses across the leakage channel inlet plane using the experimental arrangement in Figure 4. This cannot happen because it would require flow to reverse through Manual control valve 2 against the pressure drop through the valve. The experiments are sufficient to confirm the significant net overall leakage reductions that can be achieved by applying the fluid curtain, but it is not possible to demonstrate the optimum curtain flow condition in the tests.

The experimental results are backed up by CFD predictions in Figure 6. The CFD predictions were carried out with ANSYS Fluent version 15.0.7.2D using unstructured meshes created using Pointwise Version 17.3 release 5 for each geometry simulated. The calculation domains used a constant leakage channel height (b). The fluid curtain thickness (a) and seal fin clearance (c) were changed when creating meshes with different values of dimensionless parameters A and C. The full leakage channel domain used in the CFD calculations extended 70 channel heights in both directions from the labyrinth seal fin. Figure 7 shows a typical mesh in the region of the fluid curtain and labyrinth seal fin. The leakage channel inlet and outlet boundaries in the CFD calculations were sufficiently

distant from the fluid curtain and labyrinth fin to allow uniform boundary conditions to be specified without influencing the predicted interaction between the fluid curtain and the flow past the labyrinth fin. Mesh dependency was checked and it was established that 780,000 cells was sufficient to achieve mesh independent results for the range of geometries under investigation. Further details of the CFD calculations and the boundary conditions used are given in Table 1.

Cell count	~780 000
Simulation type	RANS steady state, pressure based.
Format	2D, planar.
Turbulence model	k-epsilon realizable.
Wall functions	Fluent enhanced wall treatment, y+ ~ 1.
Channel inlet boundary	Pressure inlet. Total pressure = 1.5 bara.
Channel outlet boundary	Pressure outlet. Static pressure = 1.0 bara.
Curtain inlet boundary	Total pressure increased from PR=1.0 in 0.5 steps

Table 1: Details of the CFD Calculations and Boundary Conditions used.

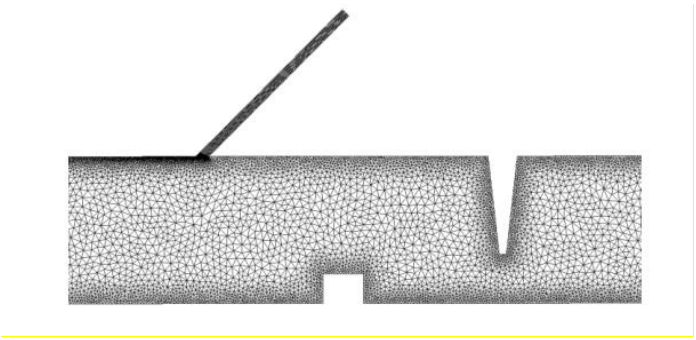

Figure 7: A typical section of unstructured CFD mesh in the region of the fluid curtain and labyrinth seal fin (A=16 and C=3 in the example shown).

The principal mechanism by which the presence of the fluid curtain influences the flow through the seal is caused by the momentum of the curtain flow opposing the flow along the leakage channel. This is an inviscid effect and so it was not necessary to use a high-order turbulence model in the CFD calculations. A two-equation k-epsilon turbulence model with wall functions was used as it was not necessary to capture the near-wall flow behaviour in fine detail.

The test results in Figure 6 validate the CFD predictions with good agreement between the experimental data and the predictions in all cases. The CFD calculations extend beyond the value of PR needed to achieve optimum (zero leakage channel inlet flow) sealing, hence the negative values for the seal inlet flow at the highest values of PR shown in Figure 6. This is important as the intersection between the predicted seal inlet flow and the x-axis in Figure 6 indicates the point of maximum total leakage flow reduction. The values of PR and L at this condition were interpolated from the CFD results for each combination of A and C investigated. All the calculations were carried out with D = 2.

Sets of CFD calculations were carried out for 90 different combinations of parameters A and C. These parameter combinations are indicated by the black crosses in Figure 8. Each set of CFD calculations was used to identify the values of PR and L at which minimum total leakage flow (i.e. zero seal inlet flow) occurred for that combination of A and C. These 90 data points for PR and for L were then used to construct the contour plot shown in Figure 8. The coloured contours indicate the leakage reduction achieved due to the presence of curtain flow at its optimum value of PR which is indicated by the black contour lines in the figure.

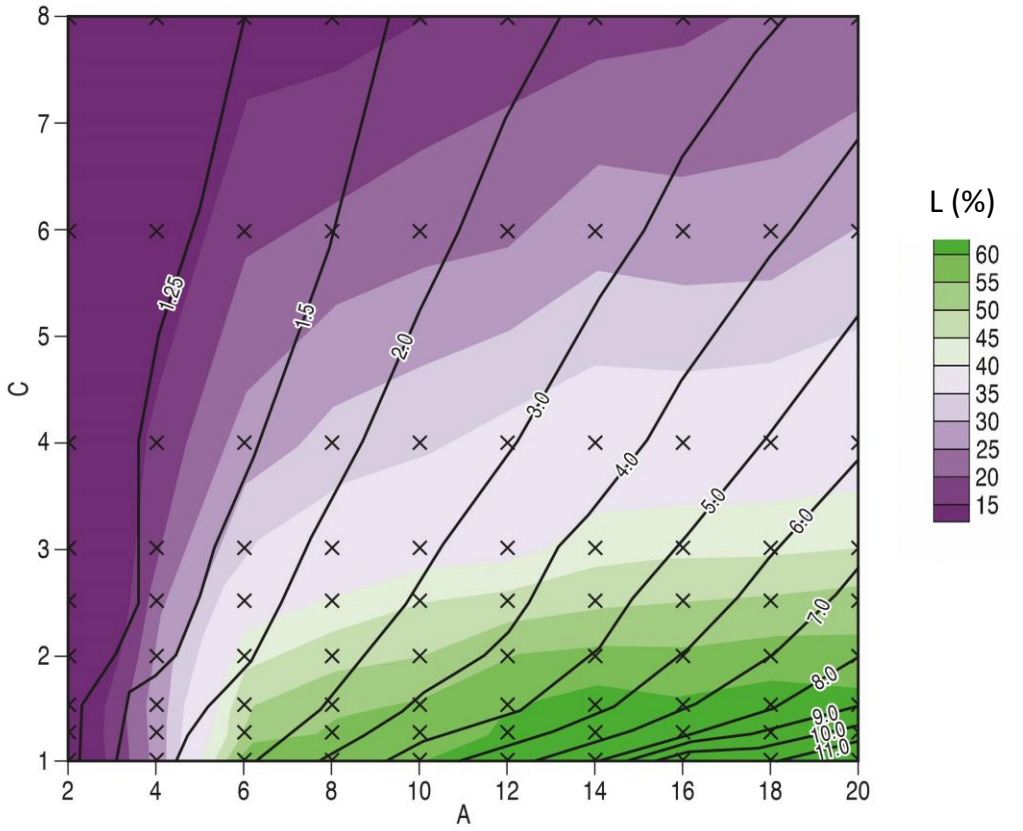

Figure 8: Fluid Curtain Seal Performance (Leakage Reduction Factor L expressed as %) over the Range of Values of A and C Examined (Values of PR needed to achieve optimum sealing indicated by black contours).

Figure 8 shows that the curtain flow can reduce leakage by 50% or more over a wide range of values of dimensionless parameter A (channel height divided by curtain flow thickness at entry), but that relatively low values of C (channel height divided by seal effective clearance) are needed for best performance. It can also be seen that as the curtain thickness decreases (i.e. A increases), the value of PR needed to achieve optimum sealing performance increases.

Some CFD calculations were carried out with a reduced axial spacing between the curtain entry plane and the labyrinth fin (D=1). These showed that the performance benefit from applying the curtain can be greatly reduced if the curtain inlet plane is too close to the labyrinth restriction.

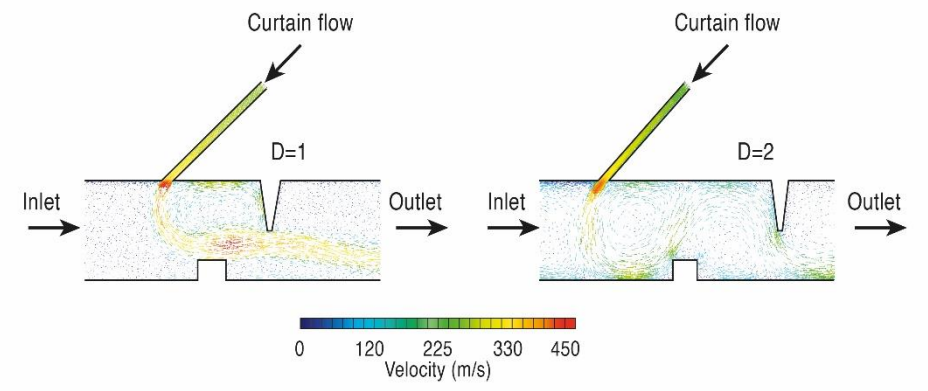

Figure 9: Velocity Vectors of seal flow for A = 12, C = 2 at PR = 6.0 with Different Values of D.

The velocity vectors are compared in Figure 9 for the idealised seal geometry with the same values of parameters A, C and PR, but for D = 1 and D = 2. In order for the curtain flow to be successful in improving sealing performance it is essential that it is able to traverse the leakage channel and impinge on its opposite wall, as happens in the right-hand vector plot in Figure 9 for D = 2. In the vector plot for D = 1 on the left-hand side of Figure 9, the presence of the kinetic energy blocker prevents this from happening. As a result, a jet of high kinetic energy curtain flow is directed straight through the clearance under the labyrinth restriction. The calculation results showed that this has a huge adverse impact on sealing performance.

Increasing D to values above 2 would not be expected to have any significant impact on the performance of the seal. The air curtain flow acting to affect a pressure drop in the upstream section of the leakage channel and the downstream seal represented by the single restriction labyrinth in the idealise geometry, can be viewed as two independent elements of the sealing system. Providing that the air curtain is sufficiently far upstream from the labyrinth seal to avoid any kinetic energy

carry-over of the curtain flow of the type seen for D = 1 in Figure 9, the sealing performance should be effectively insensitive to the value of D.

The results in Figure 8 essentially form a design tool giving an indication of the potential leakage reduction that can be achieved for any selected values of geometric parameters A and C and the value of PR needed to achieve this, for seals that include a fluid curtain with D > 2 and which comply with the seven constraints listed at the start of this section of the paper.

Effect of Swirl in the Leakage Channel Inlet Flow on Fluid Curtain Performance

As was noted in the Introduction, the presence of swirl in leakage flow often has a detrimental effect on some aspect of performance for many different types of seal. In this second part of the paper, results are described from tests carried out on another test rig to investigate the effect of swirl in the leakage flow on the fluid curtain flow. The test conditions and test seal geometry were subject to the same set of constraints as those listed at the start of the previous section, with the exception of constraint 7 'Zero swirl conditions'.

The test rig used in the second set of tests was a modification of an existing turbomachinery seal development test facility described in [17]. The modified test rig is shown in Figure 10.

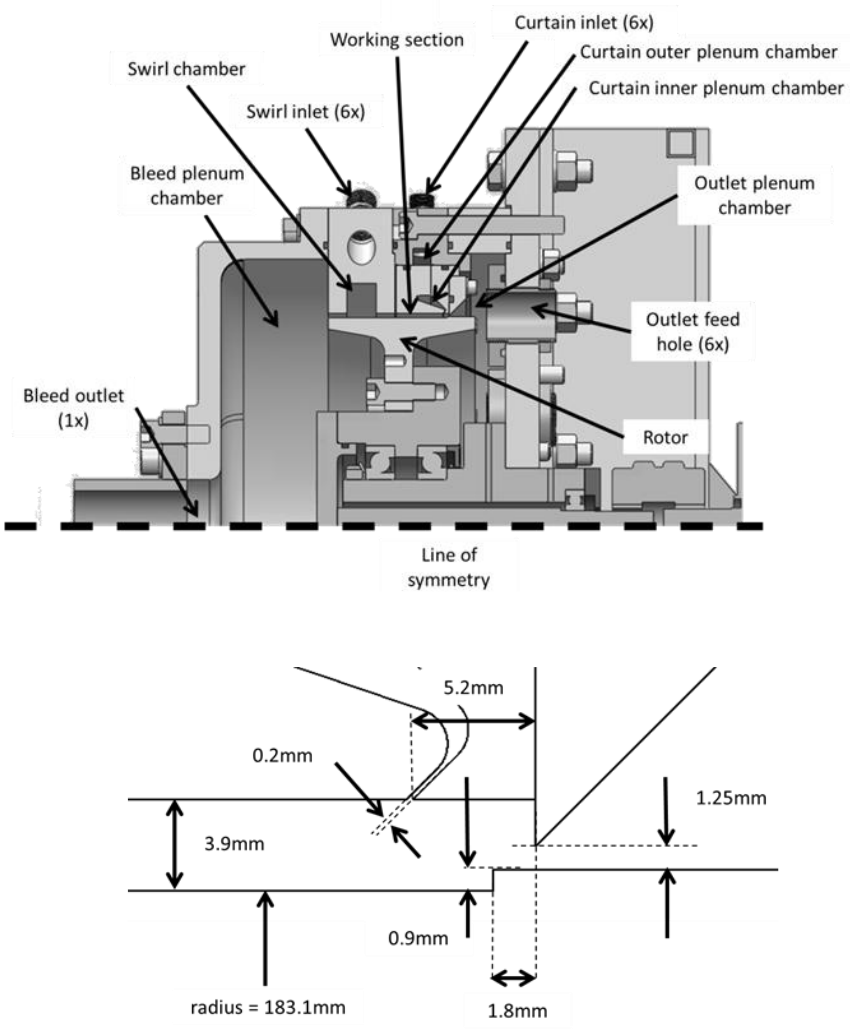

Figure 10: Cross-Section of the Test Rig and Diagram of the Working Section used to Investigate the Impact of Inlet Swirl on the Fluid Curtain.

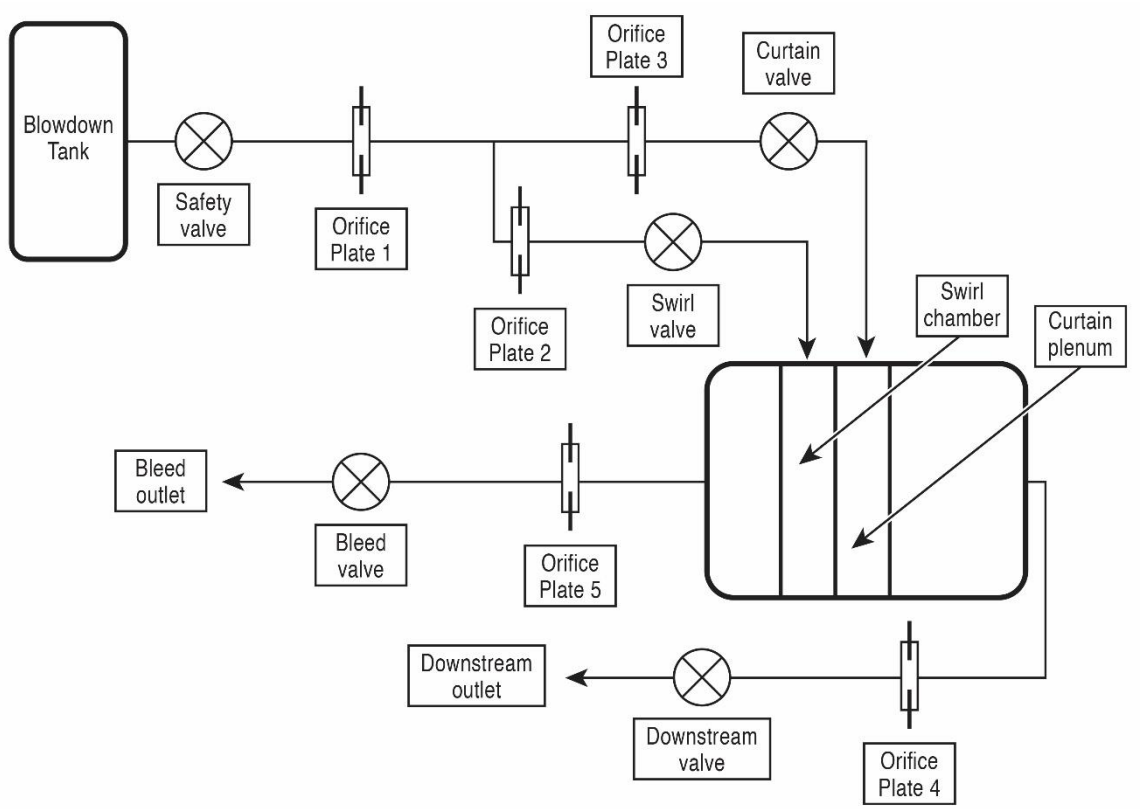

Figure 11: Schematic Diagram of the Test Rig Installation for the Tests with Swirling Inlet Flows.

The test rig was supplied from the Durham Blowdown Facility using the configuration shown in Figure 11.

The test rig featured a 366.2 mm diameter over-hung steel rotor powered by an electric motor (not shown in Figure 10). The working section featured the same generic features as the idealised seal geometry incorporating a fluid curtain used in the static rotor tests and shown in Figure 3. In this test rig, the working section again included a fluid curtain inclined at 45 degrees to the leakage flow upstream of a single restriction labyrinth seal. The kinetic energy blocker in this design took the form of a step increase in rotor diameter between the curtain inlet plane and the labyrinth seal. A sketch of the working section with dimensions is also shown in Figure 10. Table 2 gives the values for the

dimensionless geometry of the test seal design and its expected performance according to Figure 8 under no inlet swirl conditions.

Dimensionless curtain thickness, A	= b/a = 3.9/0.2 = 19.5
Dimensionless labyrinth fin clearance, C	= b/c = 3.9/1.25 = 3.12
Dimensionless Fluid Curtain to Fin Spacing, D	= d/b = 5.2/3.9 = 1.33
Leakage Channel Radius Ratio	= (183.1+3.9)/183.1 = 1.02
Expected leakage reduction factor, L (Figure 7)	0.43
Expected optimum PR (Figure 7)	6 - 7

Table 2: Test Seal Geometry and Performance from Figure 8 (No Swirl Conditions).

The test rig design included a swirl chamber (Figure 10) positioned towards the upstream end of the leakage channel. The swirl chamber was supplied by air from the blowdown tank (Figure 11) through six 19 mm diameter feed holes uniformly spaced around its circumference and inclined at 62 degrees to the radial direction. To create a large amount of swirl it is necessary to have much larger mass flow rates through the holes feeding the swirl chamber, compared to the leakage flow through the labyrinth restriction. The test rig design included a large bleed (plenum) chamber enclosing the space before the over-hung rotor (see Figure 10) to achieve this. The flow through the bleed chamber exhausted to atmosphere through the bleed pipe shown in Figure 11. The bleed pipe flow was controlled by a manually operated bleed valve. For tests with high inlet swirl, the majority of the flow through the swirl chamber exhausted through the bleed valve, with only a small portion of it forming the leakage flow through the test seal with the desired swirl inlet condition.

The flow exiting from the seal test section was collected in an outlet plenum (Figure 10) from where it exhausted from the test rig through six Outlet Exhaust Holes. The exhaust holes had flexible pipes connect to them (not shown in Figure 10) and were connected to an exhaust manifold, so that the exhaust flow exited from the test rig through a single pipe. A manual exhaust valve in the exhaust pipe allowed the leakage flow exhaust pressure in the Outlet Plenum Chamber to be controlled.

The final connection to the test rig was the curtain flow supply shown in Figure 11. This was also controlled by a manually operated curtain supply valve in a similar arrangement to that used in the static tests described in the previous section.

Five orifice plates, all designed to British Standard ISO:5167:2003, were used to measure the mass flow rates in the pipework connecting to the test facility at the locations shown in Figure 11. The pressure measurements and data logging were undertaken using the same types of instrumentation as used in the static rig tests. Appropriately rated Sensor Technics pressure transducers with accuracies of 0.2% FSO or better were used to measure the absolute and differential orifice plate pressures.

A swirl probe was positioned in the leakage channel upstream, of the fluid curtain, to obtain a direct measurement of the swirl in the leakage flow as it approached the seal. The swirl probe consisted of a section of 1.1mm diameter hypodermic tube sealed with epoxy resin at its open end and flattened on one side with a 0.2mm hole drilled through the flat face. As shown in Figure 12, the hypodermic tube was mounted on a 5 mm diameter support shaft. The shaft was mounted through the test rig casing to the outer wall of the working section, so that the end of the support shaft was flush with the wall of the leakage channel and the pressure tapping in the hypodermic tube was at channel mid-height. The support shaft was able to rotate in its mounting through the test rig casing and was attached to a stepper motor on the outside of the test rig. Flexible tubing was used to

connect the open end of the hypodermic tube to a pressure transducer. A wall static pressure tapping was also included on the outer wall of the leakage channel at the same axial location as the swirl probe but circumferentially spaced from it by 25 mm. Swirl in the seal inlet flow was measured by rotating the probe with the stepper motor to find the position where the maximum pressure was measured at the tapping in the hypodermic tube. This will be the case when the probe is aligned with the swirling flow in the leakage channel. The pressure measured at the tapping will be the total pressure of the inlet flow. The swirl angle can be deduced from the orientation of the probe and the magnitude of the inlet velocity vector calculated from the total pressure and wall static pressure measurements.

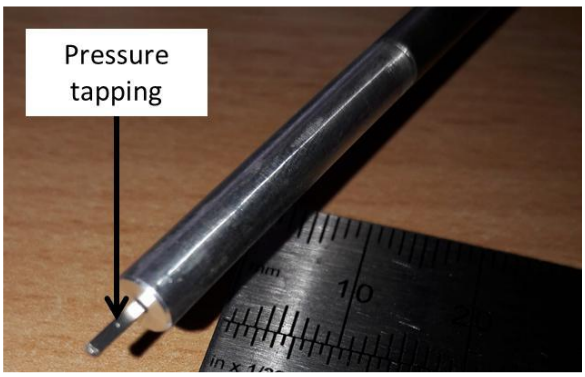

Figure 12: Tip of the Swirl Probe Showing the Total Pressure Tapping in the Side of the Hypodermic Tube.

A first set of tests were carried out on the rotating test rig with no swirl in the test seal inlet flow and a with the rotor stationary to benchmark the test results for the seal design in Figure 10 against the earlier results from the static test rig shown in Figure 8. The test rig was reconfigured for these tests so that the swirl chamber was essentially bypassed. This was achieved by removing the six supply lines from the swirl chamber inlet pipes and blanking these off. The bleed outlet pipe (Figure 11) was removed and a manifold, with the six supply lines originally from the swirl generator connected to it,

was bolted to the bleed plenum chamber in place of the outlet pipe. In this configuration, non-swirling air was supplied to the leakage channel inlet by supplying air in the reverse direction through the bleed plenum chamber effectively using it as an inlet plenum to supply the leakage channel flow.

The nominal test conditions used in the zero inlet swirl tests were inlet flow total pressure 2.0 bara and leakage channel exhaust static pressure to 1.8 bara. Similarly to the testing described in the previous section, it was not possible to set the leakage channel supply, curtain supply and leakage channel exhaust pressures precisely to the desired values during testing. The data was again corrected during post-processing using bilinear interpolation to produce a data set with a fixed leakage channel pressure drop of 0.2 bar (i.e. $p_{0,inlet}$ = 2.0 bara & p_{outlet} = 1.8 bara) and a desired range of values for PR in fixed increments. The corrected test data are shown in Figure 13.

The data in Figure 13 displays identical general trends to the data shown in Figure 6 from the earlier tests. Similarly to the previous testing, with the new test rig configured for zero swirl testing it was not possible to run tests at or beyond the optimum value of PR, where the inlet flow into the leakage channel is reduced to zero or reverses. The solid and broken lines added to Figure 13 that extrapolate the data trends beyond the optimum sealing condition are for illustrative purposes only. They underline that the test data is consistent with the expected results for optimum seal performance that are given in Table 2 based on the performance map in Figure 8. It should be noted that in these tests, the leakage channel height and radius ratio, spacing distance D and the geometry used to prevent kinetic energy carry over from the curtain flow, are all different to those in the earlier CFD and testing used to create Figure 8. This result supports the generality of Figure 8 provided that the seven constraints listed in the previous section are adhered to. The results also show that the geometric shaft feature used to block kinetic energy carry over in the latest tests is effective at values of D below 2

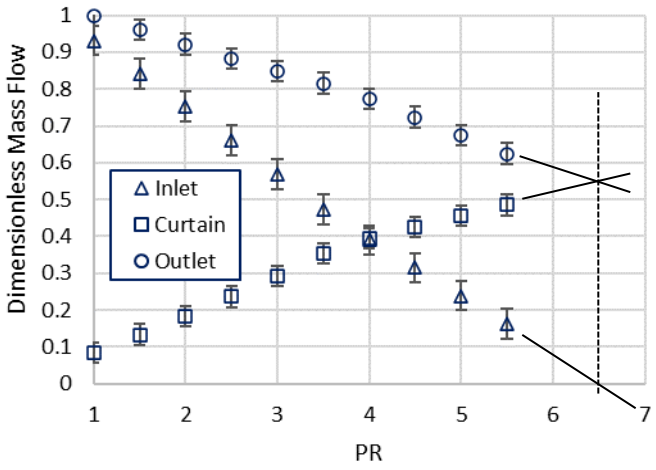

Figure 13: Dimensionless Mass Flow Rates .vs. PR for the Tests Without Inlet Swirl (extrapolation lines added for illustrative purposes).

Following the validated of the test section against previous results for no swirl conditions, the rig was reconfigured for tests with swirl by restoring the connections to the swirl chamber and the bleed outlet pipe. A series of test were carried out with the same nominal values for leakage channel inlet and exhaust pressures ($p_{0,inlet}$ = 2.0 bara & p_{outlet} = 1.8 bara). The values for $p_{0,inlet}$ used to calculate PR (Equation 4) in the swirl tests was adjusted by subtracting the swirl dynamic pressure from the measured total inlet pressure before calculating PR. This was done because the denominator in Equation 4 should be the inlet to exit pressure difference along the leakage channel that will drive flow along it. Only the dynamic pressure associated with the axial component of velocity in the inlet flow has the potential to contribute to this driving pressure drop. All the swirl tests were carried out with a nominal dimensionless fluid curtain supply pressure of PR = 6 calculated in this manner. Tests were run with swirl velocities in the inlet flow of up to 70 m/s. The rotor speed was 1,500 rpm in all the tests giving a rotor surface velocity of 28.8 m/s. This rotor speed was selected as it gave a rotor surface velocity that was close to half that of the maximum swirl velocity used in the tests, which reduced any impact of rotor surface shear on the swirl in the leakage flow. This effect is known to be small though. For example, Wasilczuk et. al. [8] demonstrate negligible effect of rotor surface speed in their air curtain seal tests.

The values for driving pressure drop along the leakage channel measured in the tests were in the range 0.11 bar to 0.28 bar and the measured values of PR in the tests ranged from 5.20 to 6.13. The added complexity of needing to correct swirl velocity meant that it was not possible to apply similar bilinear interpolation to that used previously on data from tests without swirl, to correct the data with swirl to nominal conditions.

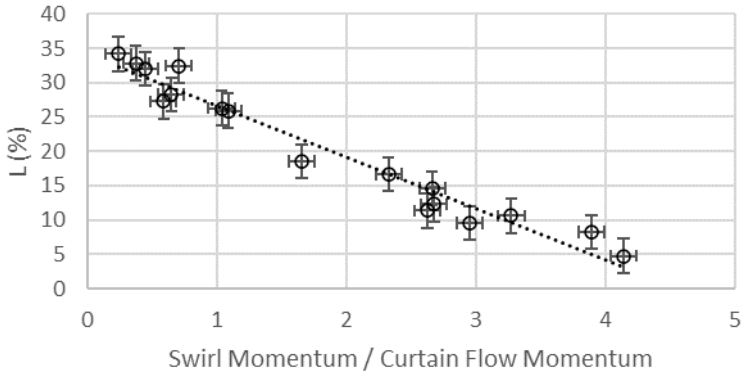

Figure 14: Mass Flow Rates .vs. PR for the Tests With Swirl (Error bars indicate measurement uncertainty).

Data from the tests with swirl is presented in Figure 14. Leakage reduction factor, L, due to the presence of curtain (Equation 5) is plotted against the ratio of the swirl momentum in the inlet flow divided by the curtain flow momentum at its point of entry into the leakage channel. These quantities are defined in Equations 6 and 7. The scatter in the data is mainly the result of the variation in PR noted above. Measurement error bars and a trendline have been added to the figure which indicate a linear decrease in leakage reduction performance with the momentum ratio lying within the band of experimental uncertainty. The variation in the driving pressure drop along the leakage channel also noted above should not have a significant impact on the scatter in the data when plotted in this dimensionless form.

$$Inlet\ Flow\ Swirl\ Momentum = (\dot{m}v_{swirl})_{inlet} \quad (6)$$

$$Curtain\ Flow\ Momentum = (\dot{m}v_{absolute})_{curtain} \quad (7)$$

Despite some scatter in the data the results in Figure 14 show a clear trend of reducing fluid curtain effectiveness as the swirl level increases. Good leakage reduction due to the curtain is achieved in tests where the inlet flow swirl momentum is less than the momentum of the curtain flow, but once this ratio gets beyond 4 any benefit due to the presence of the curtain flow is essentially eliminated.

Finally, extrapolating the data in Figure 14 by eye to zero inlet swirl indicates a value for L of between 35% and 40% with no swirl present. This is slightly lower than the expected value of 43% from Table 2 and confirmed by the data in Figure 13. A value of PR of approximately 6.5 is needed to achieve optimum sealing with this test geometry, whereas the data in Figure 14 is for a range of values (PR between 5.20 and 6.13) that are slightly below this, as already noted. This accounts for the slightly lower value for L at the zero-swirl condition indicated by the data in Figure 14 compared to the earlier results with optimum sealing.

Conclusions.

The results described in this paper demonstrate how fluid curtains injected into leakage flow paths upstream of conventional turbomachinery seals can act to reduce the total flow at exit from the leakage path. CFD calculations carried out on an idealised seal geometry which have been validated against experiments have been used to create a parametric leakage reduction performance map and guide to optimum curtain supply pressure for different curtain flow thicknesses and effective clearances of conventional seals. The leakage reduction performance map is suitable for application to seal designs where the leakage channel is cylindrical with low radius ratio, the curtain is upstream

of the conventional seal and angled at 45 degrees opposing the channel flow, the working fluid is air at 20 degrees Celsius, the flow in the leakage channel is low Mach number and where there is no swirl in the inlet flow.

The effect of inlet flow swirl on the performance of the curtain has been investigated in tests carried out on a separate facility for the same type of idealised seal geometry. These results demonstrate that inlet flow swirl has a detrimental effect on the ability of the curtain flow to reduce flow through the downstream conventional seal. If the swirl momentum in the inlet flow is greater than the momentum of the curtain flow into the channel, the reduction in effectiveness of the fluid curtain is significant.

Acknowledgments

The authors would also like to acknowledge and thank the EPSRC for supporting the work through Industrial CASE studentship number EP/N509140/1 in collaboration with GE Power, who also provided expert technical support to the project.

References

1. Deville, L. & Mihaï, A., 2019, 'Experimental Analysis of Small Diameter Brush Seals and Comparisons with Theoretical Predictions', ASME J. Trib., vol 141, n 1, Jan 2019, 141(1), Paper No: TRIB-17-1486. https://doi.org/10.1115/1.4040596.

2. Zhang, Y., Zhou, R. , Yin, M., Zhang, Y., Hu, H. & Cui, Y., 2022, 'Experimental Investigation on Friction and Wear Performance of C/C Composite Finger Seal', ASME J. Trib., vol 144, n 2, Paper No: TRIB-20-1382. https://doi.org/10.1115/1.4050882.

3. Jahn, I.H.J., Franceschini, G., Owen, A.K., Jones, T.V. & Gillespie, D.R.H, 2016, 'Improved Understanding of Stiffness in Leaf-Type Filament Seals', ASME J. Turbomach., vol 138, n 1, Paper No: TURBO-14-1309. https://doi.org/10.1115/1.4031579.

4. Yan, X., Dai, X., & He, K., 2022, 'Experimental Study on Rubbing Wear Characteristics of Labyrinth Seal with Trapezoidal Fins', ASME J. Trib., vol 144, n 3, Paper No: TRIB-21-1300. https://doi.org/10.1115/1.4052637.

5. Reggentin, P., Friedrichs, J., Flegler, J., McBean, I., 2020, 'Investigation of a novel pressure-actuated brush seal under hot steam conditions', J. Glob. Power Propuls., Vol 4, pp. 14–26. https://doi.org/10.33737/jgpps/117858.

6. Liu, Y., Dong, W., Chew, J., Pekris, M., Yue, B., Kong, X., 2022, 'Flow Conditioning to Control the Effects of Inlet Swirl on Brush Seal Performance in Gas Turbine Engines', Frontiers in Energy Research Vol. 9, Article 815152. https://doi.org/10.3389/fenrg.2021.815152.

7. Curtis, E.M., Denton, J.D., Longley, J.P., Rosic, B., 2009, 'Controlling Tip Leakage Flow over a Shrouded Turbine Rotor using an Air-Curtain', ASME Turbo Expo 2009, Orlando, Paper No. GT2009-59411. https://doi.org/10.1115/GT2009-59411.

8. Wasilczuk, F., Flaszynski, P., Kaczynski, P., Szwaba, R., Doerffer, P. & Marugi, K., 2021, 'Air curtain application for leakage reduction in gas turbine shroud sealing', Aerospace Science and Technology, vol. 112, 106636. https://doi:10.1016/j.ast.2021.106636.

9. Aubry, J. R., 2012, 'Non-contacting shaft seals for gas and steam turbines', DPhil thesis, University of Oxford.

10. Auyer, E.L., 1954, 'Dynamic Sealing Arrangements for Turbomachines', United States Patent 2685429, Assignee General Electric Company, USA.

11. Smile, H.J., Paulson, E.E., 1960, 'Pressurized Seal', United States Patent 2963268, Assignee General Electric Company, USA.

12. Unsworth, R.G., Burton, R.K., 1971, 'Turbines', United States Patent 3597102, Assignee English Electric Company, England.

13. Minoda, M., Inoue, S., Usui, H., Nouse, H., 1988, 'Air Sealed Turbine Blades', Assignee National Aerospace Laboratory of Science and Technology Agency, Japan.

14. Turnquist, N.A., Bruce, K.L., Cerretelli, C. & Tourigny, J.E., 2009, 'Fluidic Sealing for Turbomachinery', United States Patent US2009/0297341 A1, Assignee General Electric Company, USA.

15. Sun, D., Su, G.Z., Zhao, H., Wang, X.W., Xu, W.F. & Yang, Z.M., 2023, 'Dynamic Characteristics of Labyrinth Seal and Rotor Stability Considering Swirl Brakes', Journal of Aerospace Engineering, vol. 36, n. 5, Article n. 04023057. http://dx.doi.org/10.1061/JAEEEZ.ASENG-5110.

16. Crudgington, P., 1998, 'Brush Seal Performance Evaluation', AIAA-98-3172. https://doi.org/10.2514/6.1998-3172.

17. Messenger, A., Williams, R.J., Ingram, G.L., Hogg S.I, Tibos, S., Seaton, J., & Charnley, B., 2017, 'Demonstration of a Dynamic Clearance Seal in a Rotating Test Facility', ASME Turbo Expo 2017, Charlotte, NC, USA, Paper No. GT2017-64285. https://doi.org/10.1115/GT2017-64285.